Available online at www.sciencedirect.com
SCIENCE DIRECT®
Journal of Nuclear Materials 334 (2004) 13–27
journal of nuclear materials
www.elsevier.com/locate/jnucmat

Electrochemical characterisation of nickel-based alloys in sulphate solutions at 320 °C

J.-M. Le Canut, S. Maximovitch *, F. Dalard

Laboratoire d'Electrochimie et de Physicochimie des Matériaux et Interfaces (LEPMI), UMR CNRS-INPG 5631, ENSEEG, Domaine Universitaire, BP 75, 38402 St Martin d'Hères cedex, France

Received 17 June 2003; accepted 7 April 2004

Abstract

Nickel alloy steam generator tubes of pressurized water reactors (PWR) are sensitive to stress corrosion cracking (SCC) and the possibility of predicting SCC from electrochemical measurements is of considerable interest for nuclear industry. The electrochemical properties of several nickel-based alloys were studied at 320 °C in sulphate solutions at neutral or slightly alkaline pH from corrosion potential measurements, polarisation curves and polarisation resistance (R_p) measurements by linear voltammetry and electrochemical impedance spectroscopy (EIS). The passive layers were much more stable in neutral conditions, due to the presence of chromium oxide, and alloys 600TT and 690 showed the best passivity. R_p measurements confirmed that alloys 600TT and 690 have the lowest corrosion rates. At alkaline pH, the passivation currents were higher than those obtained at neutral pH, and the alloys showed a close behaviour. Reduction of sulphates to sulphides seemed to be possible. Results are in agreement with thermodynamic and surface analysis data of literature. The electrochemical stability did not appear to be directly related to SCC susceptibility since it varied inversely with the pH dependance of SCC in sulphate medium.

PACS: 81.05.Bx; 81.65.Kn; 81.65.Rv; 82.45.+z

1. Introduction

Stress corrosion cracking (SCC) is a form of corrosion that affects certain components of pressurised water reactors (PWR), and in particular the primary and secondary circuits of the steam generators.

This type of corrosion occurs on the secondary side, in confined zones where impurities of low volatility become concentrated because of limited water flow rates and differences in heat flows (hide-out phenomenom). Heat exchanger tubes are affected by cracking, caused by the simultaneous action of the chemical environment and the mechanical and thermal stress of the installation. Numerous studies have been performed to determine these conditions in secondary environment [1–21].

It is very important to be able to predict stress corrosion in the steam generator tubes of PWR reactors so as to guarantee the safety of the installation and to plan maintenance tasks. Information on SCC encountered in nuclear installations is reproduced in laboratories in conditions as close as possible to real operating conditions. Such measurements are generally long and costly and the possibility of predicting/anticipating SCC by carrying out electrochemical measurements is of considerable interest. In fact, some stress corrosion mechanisms involve localised dissolution of the alloy when the oxide layer cracks and are thus directly related to the electrochemical properties of the alloy [22]. Stress corrosion occurs in potential ranges where the passive

* Corresponding author. Tel.: +33-476 826594; fax: +33-476 826777.
E-mail address: suzanne.maximovitch@lepmi.inpg.fr (S. Maximovitch).

0022-3115/$ - see front matter © 2004 Elsevier B.V. All rights reserved.
doi:10.1016/j.jnucmat.2004.04.327

layers are not very stable, in particular around the Ni/NiO equilibrium and when the passivated surface is damaged by stress [10]. SCC depends on numerous factors, including the alloy composition and in particular the chromium content [6]. The tubes used in nuclear facilities are made from nickel-based (Inconel 600, Inconel 690) or iron-based (Incoloy 800) alloys. Alloy 600 has been the one most commonly used and is the most sensitive to SCC [4,5,8,10–14,18–21]. This alloy is used after its original heat treatment (600MA) or may be subjected to an additional heat treatment (600TT) to improve its stress corrosion resistance. Alloy 690, which has a higher chromium content, is only very slightly susceptible to SCC in most environments that crack alloy 600 [6,7].

On the secondary side of steam generators, earlier studies showed that in confined zones the environment was likely to become caustic with a high pH level, and most electrochemical studies have concerned this type of environment [1,18,19]. Some authors have modelled stress corrosion cracking in a caustic environment [23].

More recent analyses of secondary side environments, performed after hide-out return of the species dissolved at high temperatures, have shown the confined zones developed in SG secondary sides to be neutral or slightly alkaline sulphate environments [24,25].

In these sulphate conditions, SCC was found to decrease as the pH level was increased from pH 5–10 [26]. SCC increased with increasing sulphate concentrations and was strongly dependent on the alloy type, being high for alloy 600MA, and lower for alloy 600TT, after being subjected to additional annealing. It was lower still for alloy 800 and was not observed for alloy 690.

Combrade et al. examined the local chemistry [16,17] and showed the importance of surface films [27–29]. They showed that the presence of sulphate reduction products also promoted SCC [30]. The presence of sulphides, which are more stable than oxides, has been shown to inhibit the formation of the protective oxide layer [10]. In solutions with reducing properties, such as in the presence of hydrazine, the reduction of sulphates to sulphides and thiosulphates has been measured at high temperatures [31]. Thiosulphates are known for their depassivating effect even at ambient temperatures [32].

Far fewer studies have been performed in sulphate solutions than in caustic conditions, and aside from stress corrosion data, there are few electrochemical data available for this type of environment [33–36]. Some authors have studied the semi-conductive nature of passive layers formed at different temperatures [35] or formed at high temperatures (although the measurements were made under ambient conditions) [37] and have completed these measurements by surface analyses (Auger, ESCA, SIMS, SDL) [36–40].

The aim of the present study was to obtain better knowledge of the electrochemical properties of nickel-based alloys at 320 °C in sulphate solutions. Different nickel-based alloys were studied, with different sulphate concentrations at neutral or slightly alkaline pH. The experimental results include corrosion potential measurements, polarisation curves and polarisation resistance measurements based on the polarisation curves and using Electrochemical Impedance Spectroscopy (EIS). The results were analysed in the light of the thermodynamic stability of the alloy components and solution constituents at 320 °C [41–44], stress corrosion data [26] and the surface analyses in this type of solution [36–40].

2. Experimental conditions

2.1. Alloys studied

Several nickel-based alloys (600MA, 600TT, 690) and one iron-based alloy (800) were studied. The composition, heat treatment and microstructure of these alloys are given in Table 1. The standard, mill-annealed (MA) specimen is subjected a preliminary annealing at 1050 °C. The thermally-treated condition (TT) corresponds to an additional annealing for 16 h at 700 °C, which modifies the microstructure. This treatment promotes precipitation of carbides on the grain boundaries, which generally slows down the SCC process [6,7,18,20]. The specimens were electropolished in order to remove a cold-worked surface layer.

Table 1
Composition and properties of alloys 600, 690 and 800

Alloy	Composition (Ni, Cr, Fe/%)	Heat treatment	Grain size (μm)	Intergranular precipitation	Intragranular precipitation
600MA (mill-annealed)	76.50–16.01–6.59	1070 °C	8–9	High	Low
600TT (heat treated)	76.50–16.01–6.59	1070 °C + 16 h at 700 °C	8	Very high	High
690	59.10–28.9–10.95	1060–1080 °C 5hr at 700 °C	6–7	High	Low
800	33.70–21.5–42.79	1000 °C	8	Nil	Low to medium

2.2. Electrolyte

The electrolyte was a sulphate solution, at concentrations of 96, 5000 and 57000 ppm and with neutral to slightly alkaline pH at 320 °C ($\approx 5 <$ pH $<\approx 9.5$). Neutral pH at 320 °C is around 5.6 [45]. The solution was degassed and the final oxygen concentration was less than 10 ppb.

2.3. Cell

The tests were carried out in a Hastelloy C276 autoclave at 320 °C and 12 MPa. The working electrodes were steam generator tube sections 10 mm long and with a surface area of 3 cm^2. The reference electrode was an $Ag/AgCl/Cl^-$ electrode conditioned with 10^{-3} M KCl. The active part of the electrode was placed in a measuring compartment, at ambient temperature and at the pressure of the autoclave, connected to the experimental solution by a cooled salt bridge. The experimental potential, determined by calibration at different hydrogen partial pressures, was close to the SHE. The auxiliary electrode was made of platinum.

2.4. Electrochemical set-up

The electrochemical measurements were performed with an EG&G 263A digital potentiostat controlled by M270 and M352 software. The impedance measurements were performed with a Solartron measuring system comprising a 1287 potentiostat, a 1255 frequency response analyzer and a 1281 multiplexer.

2.5. Measuring conditions

Corrosion potential was measured after stabilisation of the potential of the specimens at 320 °C and 12 MPa. The stabilisation period ($t \approx 500$ h) probably resulted from the establishment of a passive layer up to a stationary state. This period also included the reorganisation of the surface through the disappearance of the electropolished layer.

The polarisation curves were plotted using linear potential sweep voltammetry, with a scan rate of 0.5 mV/s, from cathodic potentials toward anodic potentials after stabilisation of the specimen corrosion potential.

Polarisation resistance was measured at around the corrosion potential (± 15 mV/$E_{I=0}$) by potential linear sweep at a scan rate of 0.05 mV/s.

EIS was carried out in a floating mode, with the autoclave earthed for safety reasons. The measurements were potentiostatically controlled with an effective signal varying between 5 and 15 mV.

3. Results

3.1. Corrosion potential measurements

The corrosion potentials of the alloys (Fig. 1) measured after stabilisation correspond to mixed potentials from simultaneous oxidation of the metal elements and reduction of the electrolyte, in particular hydrogen evolution and possibly sulphate reduction. The platinum potential simply provided an indication of the redox activity of the solution. No significant differences were observed between the corrosion potential of the platinum and that of the alloys. Comparison of the corrosion potential values of the alloys with the theoretical H^+/H_2 line at $P_{H_2} = 0.2$ bar, shows that the corrosion potentials are close in acidic solution and slightly higher in alkaline solution. Apparently there is a higher hydrogen activity at alkaline pH that can be explained by a higher corrosion activity.

3.1.1. Comparison with potential–pH diagrams

The corrosion potential envelope is shown in the potential–pH diagrams [41] of the major components of the alloys at 300 °C (Figs. 2–4) and taking into account the presence of sulphurous species for Ni and Fe. In these diagrams, the potential ranges explored during plotting of the polarisation curves are represented by four vertical straight lines at pH 5, 6, 8 and 9.5.

In the potential range considered, the stable forms of nickel are metallic nickel and/or nickel oxide NiO in the absence of sulphur. According to [41], at pH >8 the oxide dissolves in the form of $HNiO_2^-$ while a more recent study [43] shows the oxide to be predominant up to pH 11. If the sulphurous species are taken into account, the oxidised form is NiS sulphide ($5 <$ pH $<\approx$ 7–7.5) or Ni_3S_2 sulphide (7–7.5 < pH $<\approx$ 9–9.5).

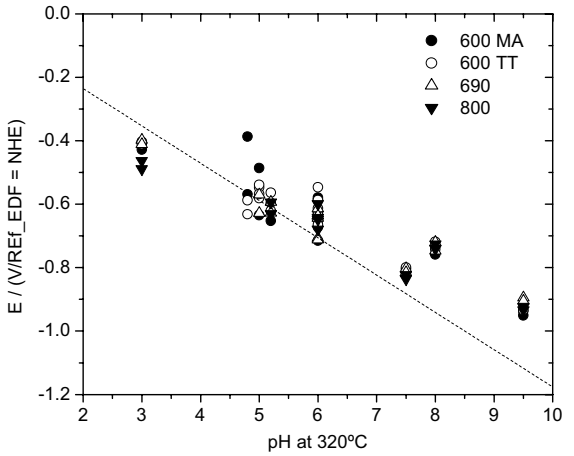

Fig. 1. Changes in corrosion potential of the alloys vs. pH at 320 °C.

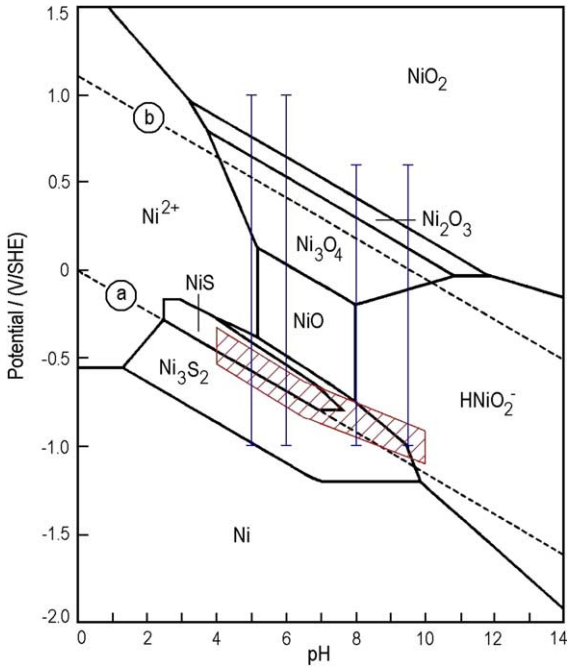

Fig. 2. Potential–pH diagram of Ni–S–H_2O system at 300 °C according to [41]. Vertical straight lines: trajectories of the polarisation curve potentials. Cross-hatched area: envelope of the corrosion potentials.

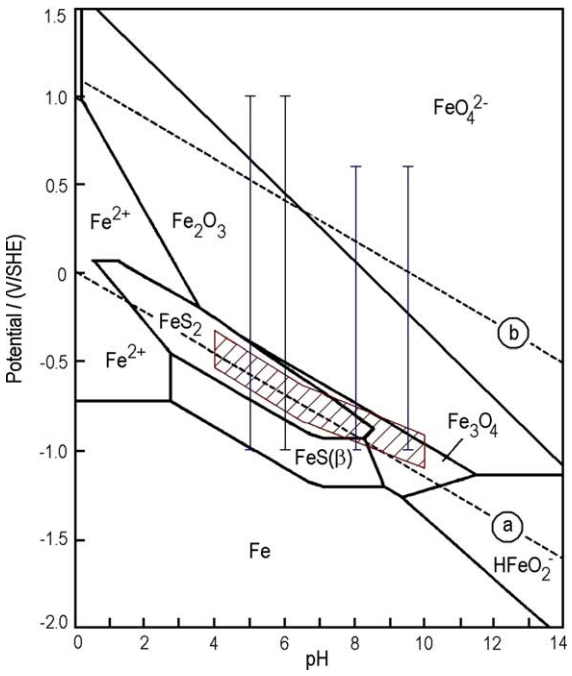

Fig. 3. Potential–pH diagram of Fe–S–H_2O system at 300 °C according to [41].

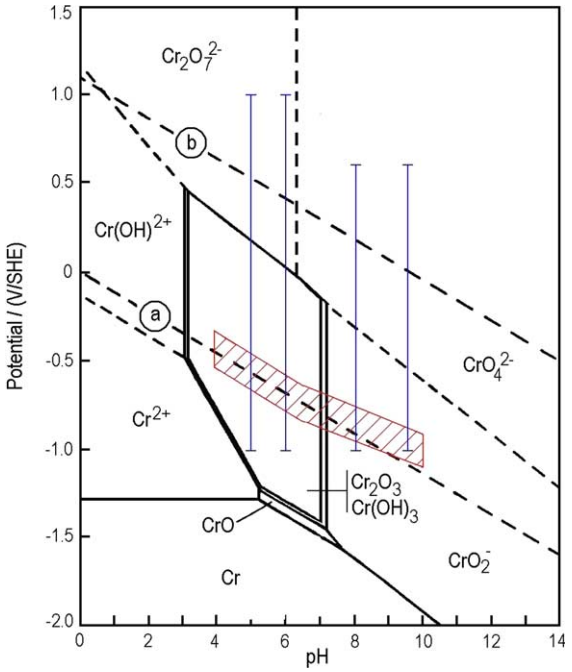

Fig. 4. Potential–pH diagram of Cr–H_2O system at 300 °C according to [41].

Direct application of the equilibrium diagrams of the chemical species must take account of the experimental conditions. Thus, the 57 000 ppm maximum sulphate concentration would represent only 5.7% of the solution concentration (0.6 M) the rest being water. In these conditions, the passive layers would almost certainly be composed essentially of oxides, with the sulphurous species inserted in the passive layer or as localised pockets.

For iron, the stable form in water is the oxide Fe_3O_4 in the pH range studied. If interaction with sulphur is taken into account, for the Fe–S–H_2O system, at pH <8.5 iron can be found in the form of FeS_2, then at pH >8.5, magnetite (Fe_3O_4) is the thermodynamically stable species.

At pH <7, the alloy equilibrium potentials are in the middle of the stable zone of the chromium oxide Cr_2O_3 or the chromium hydroxide $Cr(OH)_3$ (Fig. 4). At pH >7, the oxide (or hydroxide) is no longer stable and chromium is found in the soluble form CrO_2^-. For this element we did not take into account the interaction with sulphurous species since according to [23] chromium sulphides are not assumed to be stable in these potential and temperature conditions.

Note that the chromium and nickel diagrams have recently been recalculated [42,43]. At 300 °C, the Cr_2O_3 stable zone is extended to more alkaline pH values, as is the case of nickel, which dissolved in the form of $Ni(OH)_3^-$ at pH >11. The oxidised form of chromium

would be the hydroxide CrOOH, over a large part of the pH range [44]. There did not appear to be any dissolution in alkaline conditions, in our experiments at 320 °C, as there was at lower temperatures. This result is in agreement with that of Beverskog et al. [42] whereas the diagrams of Chen et al. [41] indicate dissolution in alkaline solutions. Other thermodynamic data for alloy 690 at 25 and 300 °C show the mixed oxide $NiFe_2O_4$ to be stable but $NiCr_2O_4$ and $FeCr_2O_4$ not to be stable at 300 °C [44].

The experimental envelope of platinum potentials measured according to pH is given in the potential–pH diagrams for sulphur (Fig. 5). This envelope is close to the stability limit of various pH-dependent equilibria: $S_2O_3^{2-}/H_2S$ (pH 5 and 6), $S_2O_3^{2-}/S^{2-}$ (at the limit of pH 8), SO_4^{2-}/S^{2-} (at the limit of pH 8 and 9.5). Reduction of the sulphates into thiosulphates and sulphides was thus possible. After the long-duration tests in 5000 and 57 000 ppm sulphate solutions, H_2S was detected when the autoclave was opened through its characteristic odour and also the platinum counter electrode was covered with a deposit which probably included corrosion products containing sulphides.

In conclusion, the alloy potentials were mixed potentials close to the H^+/H_2 equilibrium potential. For the alloys, the stability of the surface layer might depend on the pH-related stability of the chromium oxide layer. At alkaline pH, chromium oxide is soluble from pH 7 and nickel oxide from pH 8.5 [41]. Other sources show chromium oxide [42,44] to be stable up to pH 12 and nickel oxide up to pH 11. In the potential range considered, sulphur may be reduced to sulphides or thiosulphates in neutral conditions and nickel and iron to sulphides in the pH and potential range considered.

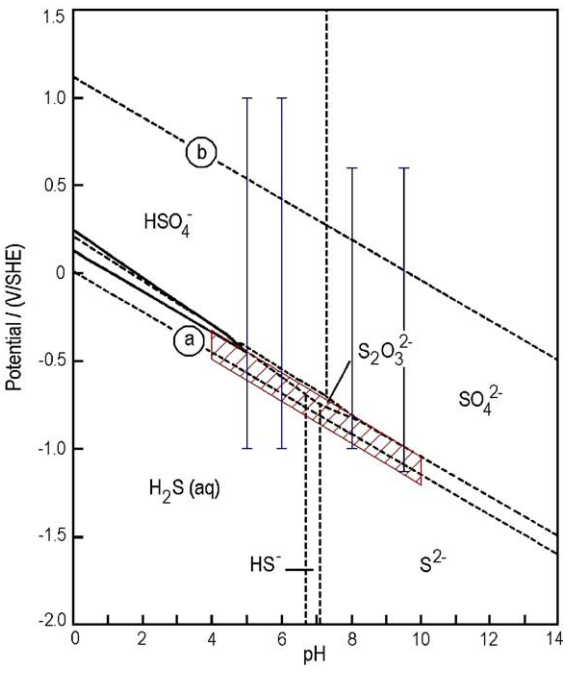

Fig. 5. Potential–pH diagram of S–H_2O system at 300 °C according to [41].

3.1.2. Comparison with surface analysis data from the literature

For PWR steam generator tubes, nickel sulphide was found by surface analysis data, in confined zones where deterioration was observed [24,25]. The presence of silicates, soluble at pH>10, was an indication of a pH below 10.

Combrade et al. investigated the local chemistry [16,17] and in particular the role of surface films [9,10, 27–29] and sulphides [30] on the passive layer [10,30], in ambient and high-temperature experiments with nickel, alloy 600 and 690.

At ambient temperature, in 0.1 N H_2SO_4, the presence of adsorbed sulphur increased the dissolution range of alloy 600 and passivation occurred at higher potentials. ESCA analyses showed that the passive film was thicker and that sulphur was present under this layer in the form of NiS. At 320 °C, in alkaline solutions, the presence of dissolved sulfides in solution totally inhibited formation of the oxide layer leading to IGA or general corrosion In neutral conditions without sulphides, surface analyses showed the underlying layer to be rich in Cr_2O_3 and the outer layer to be rich in iron. In the presence of sulphides, the surface layers analysed with ESCA after shorter experimental exposure times, were thicker but with an inner layer of Cr_2O_3 and more marked hydration than in the pure solution. Nickel sulphide and sulphates were identified, but not chromium sulphide. These layers appeared more porous, due to a corrosion process followed by deposition, rather than diffusion growth from the solid phase onwards.

The alloy chromium content was found to play an important role. In neutral conditions without sulphides, the layers became thinner with increasing Cr concentrations. This was also the case for alloy 600 in the presence of sulphides. In the case of pure nickel, in neutral solution, the sulphides totally inhibited formation of the passive layer. For alloy 600, sulphide increased dissolution kinetics. For alloy 690, they had no significant influence on the dissolution rate.

These authors concluded that on alloys 600 and 690, the presence of sulphides inhibited passive layer formation when the growth and stability of the layer were controlled by nickel oxidation (in alkaline conditions). When layer formation was controlled by chromium oxidation (in neutral conditions), the sulphides did not prevent formation of the film. They simply accelerated the dissolution rate and delayed film formation, but this effect was attenuated when the quantity of chromium

increased. Solid phase diffusion which controls the growth of a protective oxide layer was not able to produce a very protective layer and a thick, porous layer was observed.

McIntyre et al. [38] carried out an XPS study of the films formed on alloys 600, 690 and nickel alloy M400 at pH 10 in NaOH and subjected to excursions at acidic pH in H_2SO_4/NH_3. These films had a double-layered structure with an underlying layer rich in chromium and an outer layer rich in nickel and hydrated oxides $Ni(OH)_2$ and $Cr(OH)_3$. XPS revealed the presence of Cr_2O_3 and mixed oxides $NiCr_2O_4$ and $NiFe_2O_4$. In all cases, the films on alloy 600 were thick, while those on alloy 690 were very thin. These results are in agreement with those of Combrade et al. in the study described above.

In the study by McIntyre et al., for alloy 600 the presence of sulphides from sulphate reduction was confirmed throughout the entire thickness of the film by SIMS. The presence of sulphides would seem to be inversely related to chromium content since on nickel alloy M400, which does not contain chromium, the sulphide film was much thicker and seemed more permeable. Following an acid sulphate excursion and return to alkaline pH, the films appeared less protective and contained sulphides that had probably been redeposited.

Dupin et al. carried out Auger and SDL analyses of surface films formed in sulphate solution with concentrations and pH similar to our experimental conditions [39,40]. Oxide films were formed on the alloy 600 and 690 specimens immersed at 320 °C in a 57 000 ppm sulphate solution, at pH 5, 8 and 9.5, for a duration of 2250 h. The films observed on alloy 690 were thinner than on alloy 600 and they became thinner as pH increased. Chromium enrichment was more pronounced at the internal interface and decreased as pH increased: the Cr/Ni ratio was 5 at pH 5, 1.5 at pH 8 and 0.3 at pH 9.5. Oxygen was characterised by high external enrichment, which decreased over time and which might correspond to a hydrated outer layer and a less distinct internal peak In caustic solution, at pH 10, without sulphates, the layers were thinner than in the presence of sulphates, although they were still thicker on alloy 600 than on alloy 690. As in sulphate solution, a decrease in the oxygen peak was observed over time.

The sulphate concentration would seem to have influenced the structure of the films: at low concentrations (96 ppm), the films were thinner than those formed at 57 000 ppm sulphate and became thicker over time. In the case of films formed at 57 000 ppm, at alkaline pH an increase in chromium concentration was observed throughout the entire oxide thickness.

In conclusion, surface analysis data in the literature confirm that the chromium content of the passive layer decreases with increasing pH values.

Furthermore, a similarity can be observed between results obtained in low-concentration sulphate solution and sulphide-free solutions, and between high-concentration sulphate solution and media containing sulphides.

With high sulphate concentrations, or in presence of sulphide, the layers are thicker and porous, possibly due to the presence of nickel sulphides at the interface, which would tend to destabilise the passive layer. These sulphides would be the result of sulphate reduction in reducing conditions. Destabilisation becomes more marked at higher pH values and as the chromium content decreases. As the chromium content of the alloy increases, the films become thinner and the effect of the sulphides is less marked.

3.2. Polarisation curves

The polarisation curves of the alloys were plotted at pH varying from 5 to 9.5. The potential ranges explored during plotting of these curves are represented by straight line portions on the potential–pH diagrams (Figs. 2–5).

3.2.1. Neutral pH ($5 < pH < 6$)

In nearly neutral conditions at pH 5, only one passivation current plateau was observed up to oxygen evolution and no dissolution–passivation peak (Fig. 6). At pH 6, current density values were slightly lower and the beginning of a second plateau was observed around 300 mV on alloys 600MA and 600TT (Fig. 7). This plateau is much more evident in the case of alloy 690. Alloy 690 presented the lowest plateau current density, suggesting that it was more passive.

At these pH levels, and as the potential became more anodic, nickel was initially present as NiO then as Ni_3O_4

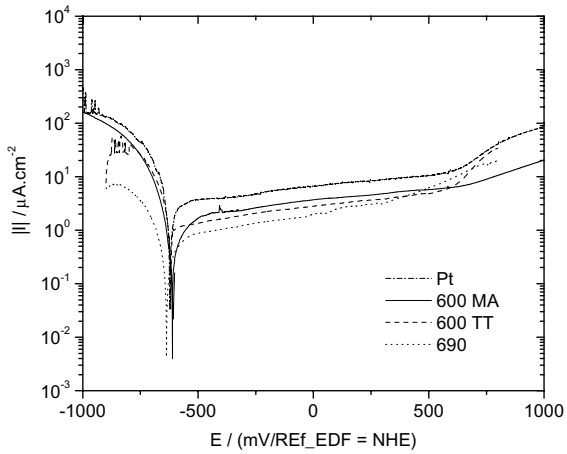

Fig. 6. Polarisation curves of alloys 600MA, 600TT, 690 and platinum at $T = 320$ °C: $[SO_4^{2-}] = 5000$ ppm, pH = 5.

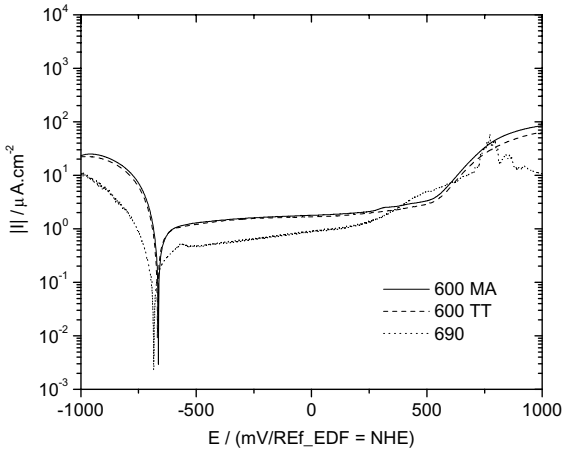

Fig. 7. Polarisation curve of alloys 600MA, 600TT, 690 and platinum at $T = 320$ °C: $[SO_4^{2-}] = 5000$ ppm, pH = 6.

and finally, at very anodic potentials, in the form of NiO_2. The absence of a dissolution–passivation peak would seem to indicate that nickel was in oxidised rather than metallic form, in the corrosion potential zone. Chromium oxide Cr_2O_3 or $Cr(OH)_3$, was stable then oxidised to $Cr_2O_7^{2-}$ at around 200 mV. The iron oxides Fe_3O_4 then Fe_2O_3 were stable and oxidised at very anodic potentials to FeO_4^{2-}. The second plateau observed at pH 6 could correspond to one of these oxidation reactions. However, it is much more likely to correspond to oxidation of Cr_2O_3 to soluble $Cr_2O_7^{2-}$ chromate. In fact, this plateau was more marked for alloy 690, which has the highest chromium content. Furthermore, chromium oxide dissolution reduced the passivity of the film, thus corresponding to an increase in current density at the second plateau, whereas in the case of nickel and iron oxidation, the oxides formed did not dissolve significantly. This hypothesis was envisaged by Olmedo et al. [34].

The passivation plateau current densities obtained by Yang [33] for alloys 600 and 690 in 15 000 ppm sulphate solutions at pH 6.5 and for alloy 800 in Na_2SO_4 2 M solution [34] are of the same order of magnitude (20 µA/cm^2). However, these authors observed a dissolution–passivation peak in the vicinity of the corrosion potential then a second plateau attributed to the transpassive zone (dissolution of Cr^{III} to Cr^{VI}). This could be due to the preliminary stabilisation conditions (over 500 h) or different surface preparations (the film is more stable on electropolished specimens). Thermodynamic data [44] show that after dissolution of the chromium, the stable surface phases should be a mixture of NiO and $NiFe_2O_4$ following loss of chromium from the oxide.

The large size of the passive part up to oxygen evolution and the low current density of the passivation plateau (1–5 µA cm^{-2}) indicate high stability of the oxide layer. This behaviour might be related to the presence of chromium oxide, which acts as an excellent barrier. The current density of the plateau depends very little on the alloy type, although the anodic plateau increased in the order 690 < 600TT < 600MA showing that alloy 690, which has the highest chromium content, was the most passive. By comparison, the slightly higher oxidation plateau observed on platinum is indicative of greater hydrogen oxidation (Fig. 6).

In the cathodic potential range explored, the nickel and iron oxides (or sulphides) might possibly be reduced, but chromium oxide was never reduced. The reduction current, corresponding essentially to H_2 evolution, was weaker for alloy 690 than for alloy 600 and platinum, possibly corresponding to a higher passivity of the chromium oxide layer.

In neutral conditions, the passive layer was thus very stable and its passivity was guaranteed by the high chromium oxide content of the passive layer, which remained stable even in the range of the cathodic potentials explored.

3.2.2. Alkaline pH (8 < pH < 9.5)

The polarisation curves at pH 8 and 9.5 are shown in Figs. 8 and 9. Unlike in neutral conditions, a dissolution–passivation peak can be observed in the region of the corrosion potential. This peak was attributed to Ni/NiO or Fe_3O_4/Fe_2O_3 reactions. It is followed by a passivation plateau with appreciably higher current densities than at neutral pH (>10 µA cm^{-2}). The passivation current density, which is higher than in neutral conditions because of the lower chromium oxide content of the passive layer [41], thus corresponds to the passivity of the nickel and iron oxides.

At higher potentials, several oxidation waves can be observed. The first at around −200 mV may correspond

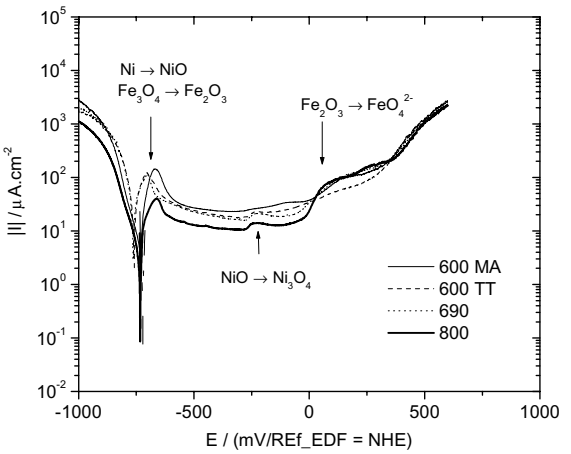

Fig. 8. Polarisation curve for alloys 600MA, 600TT, 690 and 800 at $T = 320$ °C: $[SO_4^{2-}] = 5000$ ppm, pH = 8.

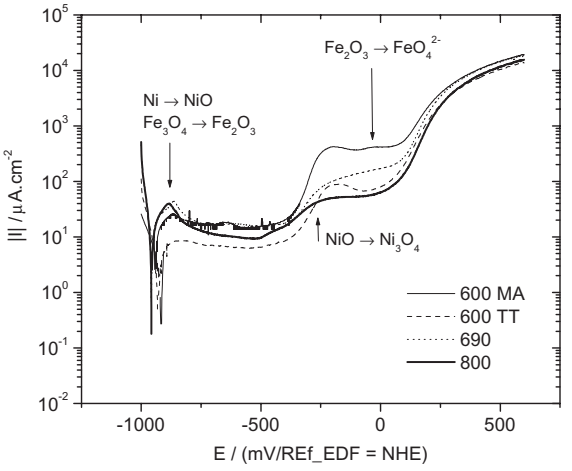

Fig. 9. Polarisation curve for alloys 600MA, 600TT, 690 and 800 at $T = 320$ °C: $[SO_4^{2-}] = 5000$ ppm, pH = 9.5.

to the NiO/Ni_3O_4 transition and the second more marked wave (at around 100 mV/NHE at pH 8, and 250 mV for pH 9.5) may correspond to the Fe_2O_3/FeO_4^{2-} oxidation reaction. In fact, at pH 8 and high potentials, the second oxidation wave is greater for alloy 800, which has a higher iron content. According to Olmedo et al. [34] this oxidation wave can be attributed to oxidation of chromium III to soluble chromium VI, which reduces the passivity of the films.

The existence of a dissolution–passivation peak, which was not observed at neutral pH, corresponds to a zone where the layers are more fragile (higher current under the peak). This is confirmed by stress corrosion tests [10].

The passive currents were similar. At pH 8, they increased in the order: 800 < 690 = 600TT = 600MA and at pH 9.5, in the order 600TT < 800 < 690 = 600MA. No trend could therefore be discerned, and it was difficult to distinguish between the materials. The good passivation properties of alloy 800 at these pH levels might be related to the greater stability of the iron oxides (nickel oxide and chromium oxide are soluble [41]). At pH 9.5, alloy 600TT did not exhibit a dissolution–passivation peak, indicating more marked passivation around the corrosion potential.

In the cathodic area, at alkaline pH, current densities were distinctly higher (from 10 to 100 times) than at neutral pH. Unlike at neutral pH, where chromium oxide cannot be reduced in this potential range and so protects the alloys, at alkaline pH levels the passive layers contain less chromium oxide, which is soluble. As shown in the diagrams (Fig. 2–5), in this potential range, sulphates can be reduced to sulphides in the form of NiS and FeS_2 or Ni_3S_2 and FeS depending on the potential. Surface analyses confirmed the presence of nickel sulphide in the surface layers and the formation of less protective porous layers in these conditions. The cathodic branch thus corresponds to reduction reactions (reduction of sulphates, H_2 evolution) and the formation of porous passive layers containing nickel sulphides.

3.2.3. Influence of sulphate concentration (96–57 000 ppm)

The influence of the sulphate content was measured at neutral pH (pH 5–6) on alloy 600MA (Fig. 10). The current density of the anodic plateau varied very little with sulphate content, which is in agreement with [34]. On the other hand, the cathodic current densities obtained at a concentration of 57 000 ppm were 10–100 times higher than those obtained for 5000 and 96 ppm, which may be related to sulphate reduction. Similar results were found for the platinum. At pH 9.5, a significant reduction current was observed at a potential higher than the thermodynamic potential of the pair ($H^+/H_2 = -1.1$ V/NHE at pH 9.5) (Fig. 9).

Surface analyses have shown that the layers formed in concentrated sulphate solutions at alkaline pH are thick and porous [39,40], as in the case of passive layers formed in the presence of sulphides [30]. These results confirm the reduction of sulphates to sulphides. According to the surface analyses, the formation of sulphides is promoted when the main constituent of the passive layer is nickel (in alkaline conditions). Nickel sulphide then forms upon contact with the metal whereas in neutral conditions it forms on an underlying chromium oxide layer [30].

3.2.4. Conclusion

The polarisation curves reveal two types of behaviour depending on pH. At neutral pH, the alloys were very passive due to the chromium oxide, while in more

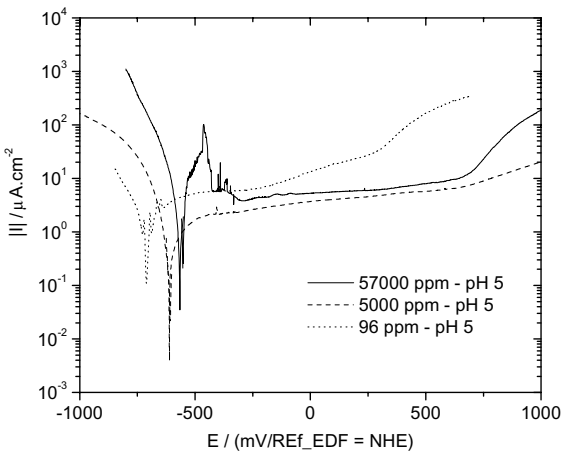

Fig. 10. Polarisation curves for alloy 600MA with different sulphate concentrations at $T = 320$ °C, neutral pH (5–6).

alkaline conditions they became less passive. Given the order of magnitude of the anodic plateaux, in the order 690 < 600TT < 600MA, alloy 690 which has the highest chromium content, was the most passive in neutral conditions. At alkaline pH, the passivity currents were similar. No trends could therefore be observed to classify the alloys. The effects of the sulphurous species were observed in the cathodic potential range. Sulphates could be reduced, at high sulphate concentrations in neutral conditions. In alkaline conditions, in the cathodic area and without chromium oxide in the passive layer, sulphate reduction was facilitated. These results confirm those from of surface analyses in the literature.

3.3. Polarisation resistance

Polarisation resistance indicates the different reaction rates at the corrosion potential: for the platinum electrode, immune to chemical attack, redox reactions of hydrogen and sulphurous species, and for the alloys, redox reactions at the surface and alloy dissolution–passivation reactions. In the presence of redox systems, polarisation resistance therefore does not simply characterise corrosion reactions.

3.3.1. Neutral solution

In neutral conditions and with a low sulphate concentration (96 ppm), the polarisation resistance of the specimens was low for $t < 300$ h, then increased considerably before stabilising when $t > 400$ h (Fig. 11). For long time durations, the polarisation resistance values were higher for the alloys (50–160 $k\Omega\,cm^2$) than for the platinum (20 $k\Omega\,cm^2$). These values provide a measure of the redox and corrosion kinetics, which overall were slow in the passive layers. In the presence of a small quantity of sulphates, the passive layer must be mainly composed of oxides.

In the case of the platinum, assumed to be immune to corrosion, the low R_p value corresponds to faster redox kinetics. This activity was probably due to the preponderant effect of the reversible H^+/H_2 reaction since the medium contained few sulphates that could be reduced and few corrosion products from the alloys that could be deposited on the platinum electrode.

When the sulphate concentration was increased (5000 ppm), no clear time-related R_p transition could really be observed, but data were unavailable for short durations. At pH 5 (Fig. 12), alloy 690 first exhibits a transition (500 h) then R_p increases linearly with time before stabilising after 1900 h. The polarisation resistance of alloy 600TT increases linearly whereas alloy 600MA exhibits a low, very constant value. At pH 6 (Fig. 12), the tendencies are more varied. The polarisation resistance is lower for alloys 600MA and 800 than for alloys 600TT and 690. High values were observed for short time durations, and these decreased after 300–400 h then increased with time. These values could be the signature of an oxide layer formed on an electropolished layer, which first exhibited good corrosion resistance and then

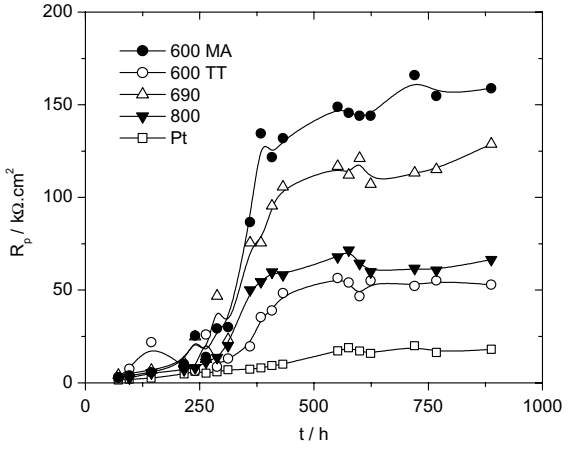

Fig. 11. Changes in R_p vs. time: $[SO_4^{2-}] = 96$ ppm, pH = 6.

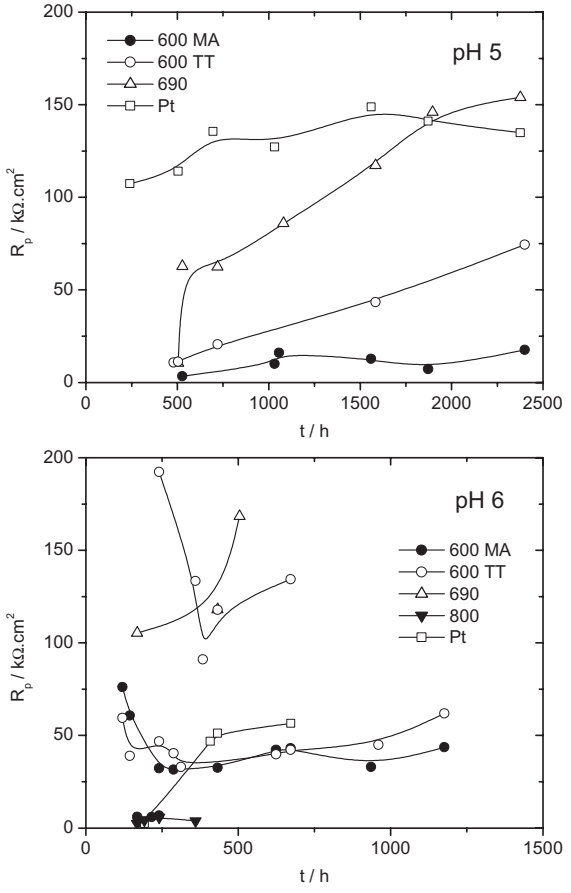

Fig. 12. Changes in R_p vs. time: $[SO_4^{2-}] = 5000$ ppm, pH 5–6.

became the seat of greater corrosion after reorganisation of the oxide layer.

Repeated tests in the same conditions yielded significantly different R_p values: 5 and 30 $k\Omega cm^2$ with alloy 600MA and 30 and 120 $k\Omega cm^2$ with alloy 600TT. It was concluded that these measurements were not sufficiently repeated to allow a precise comparison of the alloys.

3.3.2. Alkaline solution

At alkaline pH levels, polarisation resistance values were lower than at neutral pH, indicating that the layers were less passive. The lowest values were found at pH 8 (<5 $k\Omega cm^2$) (Fig. 13). At pH 9.5, polarisation resistance values were low up to 1000 h then increased while remaining below 30 $k\Omega cm^2$ (Fig. 13). This result is in agreement with the polarisation curves, which exhibited a higher plateau in alkaline conditions. Near the corrosion potential, the dissolution current under the dissolution–passivation peak was high. For these alkaline pH levels, the alloy oxide layers were less passive due to the solubility of chromium oxide, as noted before.

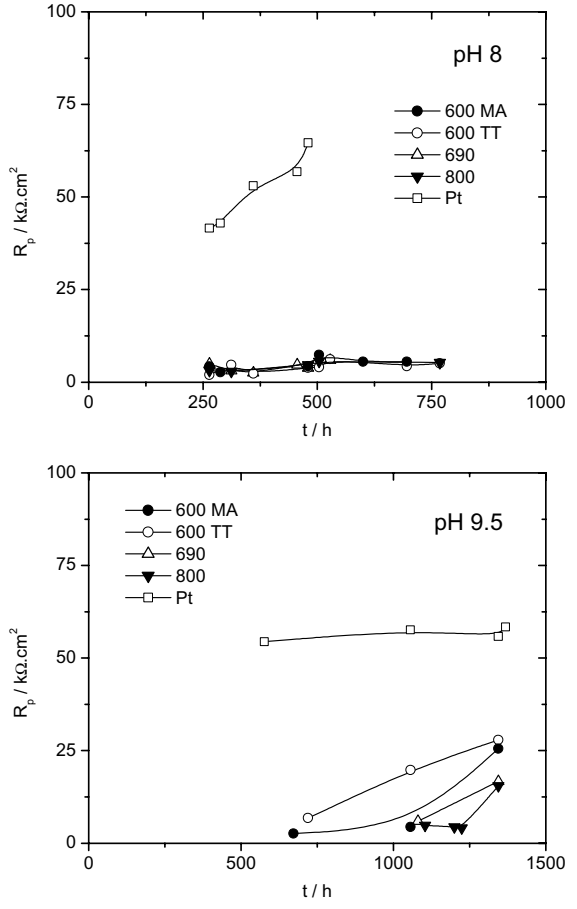

Fig. 13. Changes in R_p vs. time: $[SO_4^{2-}] = 5000$ ppm, pH 8–9.5.

3.3.3. Sulphate concentration

The polarisation resistance values for the alloys did not appear to be related to the sulphate concentration. In the neutral pH range, the values were high (160 $k\Omega cm^2$) at the two concentrations studied (96 and 5000 ppm) (Figs. 11 and 12). However, it is difficult to draw a reliable conclusion because of the lack of sufficient data for high and low concentrations.

For the platinum electrode at long time durations ($t > 500$ h), polarisation resistance was lower for the 96 ppm sulphate solution (20 $k\Omega cm^2$) than for the 5000 ppm sulphate solutions at different pH levels. In the latter case, R_p exhibited comparable values at pH 6, 8 and 9.5 (50–60 $k\Omega cm^2$) and a higher value at pH 5 (130 $k\Omega cm^2$). R_p was thus dependent on the sulphate concentration, with pH having little influence. The highest value obtained at pH 5 indicates that the redox reactions were probably slowed down by increased deposition of corrosion products.

3.3.4. Conclusion

The R_p measurements simply indicate a trend since the values are not sufficiently precise and/or reproducible for the materials to be classified definitively. For example, alloys 600MA and 600TT, in low concentration neutral pH solution, exhibited behaviour opposite to that in the other tests.

A comparison of the most numerous tests performed in 5000 ppm sulphate solution reveals that alloys 600MA and 800 exhibited the highest corrosion rate ($\propto 1/R_p$) and alloys 600TT and 690 the lowest corrosion rates (Fig. 14). The corrosion rate of the alloys was much faster at pH 8 and 9.5 than in neutral pH conditions, which is in agreement with the polarisation curves. Electrochemical impedance spectroscopy was performed to further clarify the kinetic results obtained by linear polarisation.

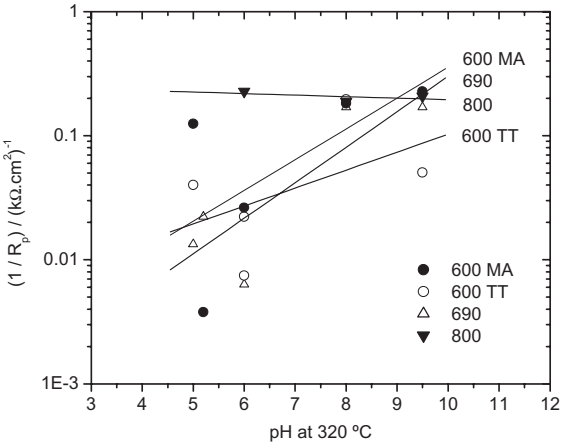

Fig. 14. Changes in $1/R_p$ vs. pH: $[SO_4^{2-}] = 5000$ ppm, 700 $h < t < 1000$ h.

3.4. Electrochemical impedance spectroscopy (EIS)

EIS measurements were performed at the corrosion potential, in neutral conditions (pH 6) with low sulphate concentration (96 ppm) and at different immersion times corresponding to the conditions in Fig. 11: at the start of the test (95 and 120 h), when the corrosion rates were high, then at the start of transition (330 h) and at end of transition (380 h). This last measurement was close to long term stationary behaviour.

The experimental impedance diagrams are given for each specimen in Figs. 15 (short times) and 16 (long times). Characteristic frequencies are shown as frequency logarithm. The Nyquist diagrams show several arcs corresponding to different immersion times.

3.4.1. Alloys

In the case of the alloys, for short immersion times, a high frequency arc (100–1 kHz), a medium frequency arc (1–10 Hz) and part of a low frequency arc (10–0.1 Hz) can be observed. The diagrams for alloys 600MA, 690 and 800 were similar, while alloy 600TT exhibited higher impedance values and a more distinct medium frequency arc.

For longer immersion times, the resistance associated with the high frequency arc increased (from 1–2 to 5–20 $k\Omega\,cm^2$) and the characteristic frequency of this arc decreased (from 10–70 to 1–5 kHz). Fig. 16 shows the change in impedance before and after the transition. Between the two measurements, the resistance of the high frequency arc increased by a few $k\Omega\,cm^2$. The most notable change concerns the medium and low frequency arcs, for which the associated resistances increased considerably by about 10 $k\Omega\,cm^2$, corresponding to a change in kinetics of the corrosion control process and formation of the passive layers. This could be interpreted as indicative of formation of a layer that has reached a certain composition and/or thickness (HF arc), which limits electrochemical reactions and material transport.

Alloys 600MA and 690 exhibited similar values of impedance, which were higher than those obtained for alloys 600TT and 800. These values confirmed the classification of the materials for long immersion times made on the basis of R_p measurements (Fig. 11). Because of the limitations of low frequency measurements, polarisation resistance could not be measured. The R_p values obtained by linear polarisation were about double the maximum EIS values. These values could

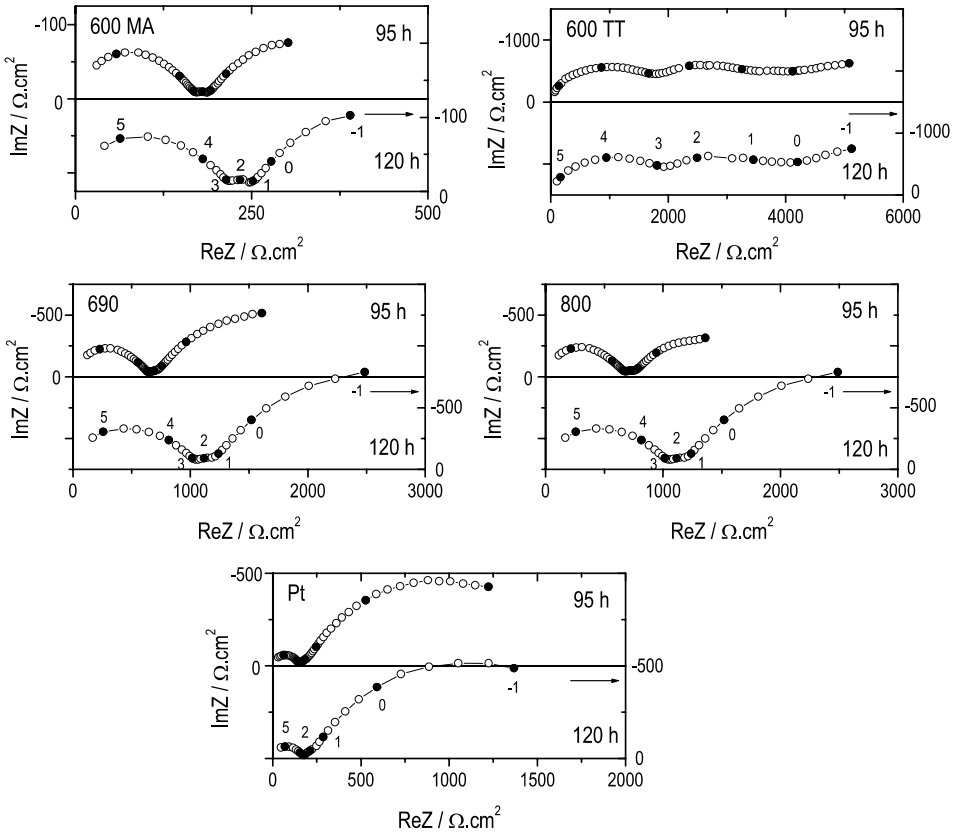

Fig. 15. Nyquist diagrams after 95 and 120 h: $[SO_4^{2-}] = 96$ ppm, pH = 6.

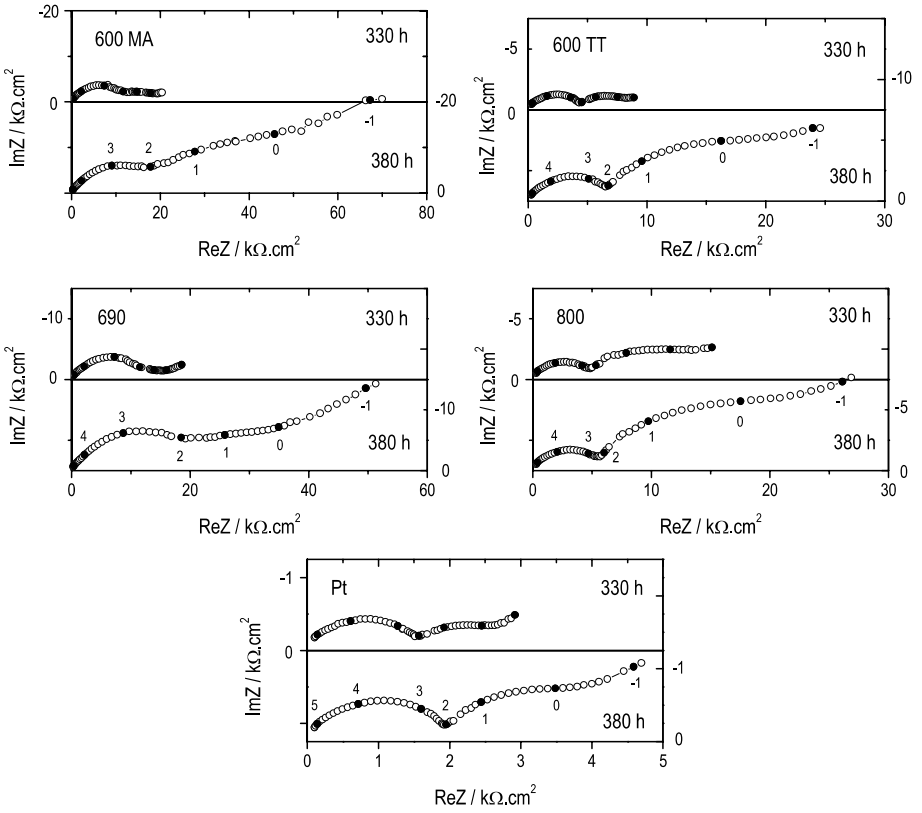

Fig. 16. Nyquist diagrams after 330 and 380 h: $[SO_4^{2-}] = 96$ ppm, pH = 6.

quite possibly correspond to the size of the low frequency arc.

3.4.2. Platinum

The platinum electrode showed only two arcs for the short immersion times. The resistance of the HF arc was lower (0.3 $k\Omega\,cm^2$) than that obtained with the alloys (1–2 $k\Omega\,cm^2$). The resistance of this arc increased with time (2 $k\Omega\,cm^2$) while remaining below that observed for the alloys.

For long immersion times at low frequencies, a straight line portion associated with a diffusional process is also visible. The shape of the impedance diagram is similar to that of the alloys.

High frequency resistance is related to surface film characteristics. As the film becomes thicker, the high frequency resistance increases. This is what was observed for both the platinum and the alloys. In the case of the alloys, the surface film was a passive layer, which corresponds to the results already obtained and to those in the literature. Platinum, being a noble metal, is assumed not to have a passive layer. The surface film in this case would be an insoluble layer possibly formed by deposition of corrosion products from the alloys over time. The formation of a platinum oxide film might also be considered, though this would be unrealistic around H^+/H_2 potential and only occurs at potentials close to oxygen evolution.

The straight line portions observed for long immersion times at low frequency and indicative of a diffusional process across this film confirm the presence of a deposit on the platinum.

3.5. Discussion

3.5.1. Thermodynamic stability and influence of pH

The electrochemical results show that pH had a significant influence on the behaviour of the alloys. The oxide layers were much more passive in neutral conditions, due to the presence of chromium oxide. At alkaline pH, when chromium oxide is soluble, the layers were less passive. Surface analysis data confirmed this hypothesis: the layers were very rich in chromium at neutral pH and contained very little chromium at alkaline pH, particularly in solutions with low sulphate concentrations.

3.5.2. Effect of sulphates

Thermodynamic and surface analysis data show that reduction of the sulphates to thiosulphates (see Fig. 5)

and sulphides was possible and that their effect was more marked when the passive layer contained little chromium oxide (in basic solution). Surface analysis showed that in solutions with a high sulphate concentration, the passive layers changed considerably, becoming thick and with chromium present throughout the entire thickness. The formation of a stable oxide layer was probably inhibited by sulphides, which were responsible for the formation of a porous layer containing nickel sulphide at the interface, as demonstrated in [10,30]. The electrochemical results confirm these data. In solutions with a high sulphate content, a higher reduction current value was observed.

3.5.3. Comparison with stress corrosion results

The polarisation curves show that in neutral conditions the most passive materials were alloys 690 and 600TT whereas in alkaline conditions the polarisation curves were not sufficiently differentiated to be able to classify the alloys.

Polarisation resistance measurements indicated that the materials could be divided into two groups: alloys 600MA and 800, with the lowest R_p values, and alloys 600TT and 690 with the highest R_p in most of the tests. Alloys 600TT and 690 thus appeared slightly more stable. The behaviour of the alloys was thus fairly comparable, whereas in the case of stress corrosion susceptibility they are clearly differentiated. Furthermore, in stress corrosion tests [26] the crack growth rate, in the order $V_{SCC}690 < V_{SCC}800 < V_{SCC}600TT < V_{SCC}600MA$ does not reflect the order of electrochemical stability.

The effect of pH may seem surprising. Indeed, it has been found that stress corrosion susceptibility increased as the pH level dropped [26] while the passive layers were much thicker and much more stable at neutral pH. In caustic conditions, unlike in sulphate solutions, stress corrosion has been found to increase with pH [23]. This result is in the inverse of the trend in electrochemical stability, given that the structure of the passive layers differs considerably depending on the presence of a low or high sulphate concentration (thick porous layers and presence of chromium).

4. Conclusion

The thermodynamic stability of the passive layers of alloys 600, 690 and 800 at 320 °C, 12 MPa, in sulphate solutions at pH 5 to 9.5, was strongly influenced by pH. The potential–pH diagrams showed that the passive layer was very stable at neutral pH levels (pH 5–6) because of the presence of chromium oxide and nickel and iron oxide or sulphide. The oxide layer was less stable at alkaline pH levels (pH 8–9.5) because of chromium oxide solubility. In accordance with these data, the polarisation curves corresponded to passivity in neutral conditions. At alkaline pH, the passivation current was higher with a dissolution–passivation peak corresponding to less stable layers.

In neutral conditions, the polarisation curves indicated corrosion rates for the specimens in the following increasing order: $V_{cor}690 < V_{cor}600TT < V_{cor}600MA < V_{cor}800$. Alloy 690, with the highest chromium content, had the lowest corrosion rate. In alkaline solutions, where the instability of the chromium oxide prevents the formation of a really protective oxide film, corrosion rates were higher and more comparable. It was therefore difficult to separate the trend in passivity of the materials.

The polarisation resistance measurements revealed distinct differences in passive film growth kinetics over time, with a high corrosion rate at the start of the test and stationary conditions for long immersion times. The specimens could be divided into two groups with opposing tendencies: alloys 600MA and 800 exhibited the lowest R_p values and alloys 600TT and 690 the highest values in most of the tests.

In the corrosion potential range measured, close to redox potential of H^+/H_2, reduction of sulphates to sulphides and/or thiosulphates seemed to be possible according to the thermodynamic data displayed on Fig. 5. Surface analysis results also confirmed that the presence of high sulphate concentrations influenced the nature of the surface layers.

These electrochemical results did not reveal a clear difference between the specimens whereas their stress corrosion behaviour is quite different. Moreover, stress corrosion resistance does not appear to be related to the passivity of the layers since an increase of passivity was observed at neutral pH when the layers were apparently in their most stable state. The electrochemical results reflected the stationary behaviour at long immersion times whereas stress corrosion involves the transient behaviour of the materials during restoration of the passive film. The question must therefore be examined in terms of transient methods and will be the subject of a second article.

Acknowledgements

The authors are grateful to Electricité De France for financial support and to O. De Bouvier, EDF, Centre de Recherche des Renardières, 77818, Moret-sur-Loing for fruitful discussion and collaboration.

References

[1] J.M. Gras (Ed.), La Corrosion côté Secondaire des Tubes de Générateurs de Vapeur, EDF/Framatome/CEA, EDF, 1996.

[2] J.M. Gras, in: S.M. Bruemmer (Ed.), Parkins Symposium on Fundamental Aspects of Stress Corrosion Cracking

Meeting Date 1991, 411-32, The Mineral Metals and Material Society, Warrendale, PA, 1992.
[3] F. Foct, O. De Bouvier, T. Magnin, Metall. Mater. Trans. A 31 (2000) 2025.
[4] D. Noel, O. De Bouvier, F. Foct, T. Magnin, J.D. Mithieux, F. Vaillant, in: T. Magnin (Ed.), Proceeding of International Conference on Corrosion–Deformation Interactions (CDI'96), Nice, France, 24–26 September 1996, European Federation of Corrosion Publications, EFC 21, 1997, p. 435.
[5] R. Rios, T. Magnin, D. Noel, O. de Bouvier, Metall. Mater. Trans. A 26 (1995) 925.
[6] F. Vaillant, J.D. Mithieux, O. de Bouvier, D. Vancon, G. Zacharie, Y. Brechet, F. Louchet, in: S. Bruemmer, P. Ford, G. Was (Eds.), Proceeding of the 9th International Symposium on Environmental Degradation of Materials in Nuclear Power Systems – Water Reactors, Newport Beach, CA, USA, 1–5 August 1999, The Mineral Metals and Material Society, Warrendale, PA, USA, 1999, p. 251.
[7] L. Guinard, O. Kerrec, D. Noel, S. Gardey, F. Coulet, J. Brit. Nucl. Energ. Soc. 36 (1997) 19.
[8] R.B. Rebak, Z. Szklarska-Smialowska, Corros. Sci. 38 (1996) 971.
[9] P. Combrade, O. Cayla, M. Foucault, D. Vançon, A. Gelpi, G. Slama, in: G.J. Theus, J.R. Weeks (Eds.), Proceeding of the 3rd International Symposium on Environmental Degradation of Materials in Nuclear Power Systems – Water Reactors, Traverse city (MI), 30 August–3 September 1987, The Metallurgical Society, 1988, p. 525.
[10] P. Combrade, P. Malagola, G. Pinard-Legry, in: Proceedings of the Conference on Water Chemistry of Nuclear Reactor Systems, Water Chemistry, vol. 3, BNES, London, 1983, p. 271.
[11] J.R. Crum, Corrosion 42 (1986) 368.
[12] R.B. Rebak, Z. Szklarska-Smialowska, Corrosion 47 (1991) 754.
[13] N. Totsuka, E. Lunarska, G. Cragnolino, Z. Szklarska-Smialowska, Corrosion 43 (1987) 505.
[14] C. Soustelle, M. Foucault, P. Combrade, K. Wolski, T. Magnin, in: S. Bruemmer, P. Ford, G. Was (Eds.), Proceedings of 9th International Symposium on Environmental Degradation of Materials in Nuclear Power Systems – Water Reactors, Newport Beach, CA, USA, 1–5 August 1999, The Mineral Metals and Material Society, Warrendale, PA, USA, 1999, p. 105.
[15] P.M. Scott, P. Combrade, in: Proceedings of the 8th International Symposium on Environmental Degradation of Materials in Nuclear Power Systems – Water Reactors, Amelia Island, FL, USA, 10–14 August 1997.
[16] P. Combrade, A.P.L. Turner, F. Cattant, S.P. Chambers, R.A. Clark, D. Gomez-Briceno, S.J. Kast, M. Rootham, S.G. Sawochka, Y. Shoda, in: R.W. Staehle, J.A. Gorman, A.R. McIlree (Eds.), Proceedings of the Meeting on Improving the Understanding and Control of Corrosion on the Secondary Side of Steam Generators, Airlie, VA, USA, 9–13 October 1995, 1996 NACE International, Houston, TX, p. 63.
[17] B. Sala, P. Combrade, R. Erre, A. Gelpi, in: R.E. Gold, E.P. Simonen (Eds.), Proceedings of the 6th International Symposium on Environmental Degradation of Materials in Nuclear Power Sysems – Water Reactors, San Diego, California, 1–5 August 1993, The Minerals, Metals and Material Society, Warrendale, PA, 1993, p. 215.
[18] K.H. Lee, G. Cragnolino, D.D. MacDonald, Corrosion 41 (1985) 540.
[19] R. Bandy, R. Roberge, D. Van Rooyen, Corrosion 41 (1985) 142.
[20] W.K. Lai, Z. Szklarska-Smialowska, Corrosion 47 (1991) 40.
[21] D. Gómez-Briceño, M.L. Castaño, M.S. García, Nucl. Eng. Des. 165 (1996) 161.
[22] F.P. Ford, in: D. Desjardin, R. Oltra (Eds.), Corrosion sous Contrainte–Phénoménologie et Mécanismes, Bombannes 1990, Les Editions de Physique, Les Ulis, 1992, p. 735.
[23] E.M. Pavageau, F. Vaillant, J.P. Caire, F. Dalard, M. Bouchacourt, in: D. Miannay, P. Costa, D. François, A. Pineau (Eds.), Proceeding of EUROMAT 2000, Tours, France, 7–9 November 2000, in: Advances in Mechanical Behaviour – Plasticity and Damage, vol. 2, Elsevier, 2000, p. 1181.
[24] B. Sala, S. Chevalier, M. Dupin, A. Gelpi, in: Proceeding of the International Symposium Fontevraud IV, France, 14–18 September 1998, Société Française pour l'Energie Nucléaire, Paris, 1998, vol. 2, p. 553.
[25] F. Cattant, M. Dupin, B. Sala, A. Gelpi, in: Proceeding of the International Symposium Fontevraud III, France, 12–16 September, 1994, Société Française pour l'Energie Nucléaire, Paris, 1994, vol. 2, p. 469.
[26] O. de Bouvier, B. Prieux, in: S. Bruemmer, P. Ford, G. Was (Eds.), Proceeding of the 9th International Symposium on Environmental Degradation of Materials in Nuclear Power Systems – Water Reactors, Newport Beach, CA, USA, 1–5 August 1999, The Mineral Metals and Material Society, Warrendale, PA, USA, 1999, p. 695.
[27] A. Machet, A. Galtayries, P. Marcus, P. Combrade, P. Jolivet, P. Scott, Surf. Interface Anal. 34 (2002) 197.
[28] A. Machet, A. Galtayries, P. Marcus, A. Gelpi, C. Brun, P. Combrade, J. Phys. IV 11 (2001) Pr179.
[29] P. Combrade, P. Scott, in; T. Magnin (Ed.), Proceeding of International Conference on Corrosion–Deformation Interactions (CDI'96), Nice, France, 24–26 September 1996, European Federation of Corrosion Publications, 1997, EFC 21, p. 394.
[30] P. Combrade, M.A. Foucault, D. Vancon, P. Marcus, J.M. Grimal, A. Gelpi, Memoires et Etudes Scientifiques de la Revue de metallurgie 87 (1990) 429.
[31] P. Kritzer, N. Boukis, E. Dinjus, Corrosion 54 (1998) 689.
[32] W.-T. Tsai, T.-F. Wu, J. Nucl. Mater. 277 (2000) 169.
[33] I.J. Yang, Mater. Chem. Phys. 49 (1997) 50.
[34] A.M. Olmedo, M. Villegas, M.G. Alvarez, J. Nucl. Mater. 229 (1996) 102.
[35] R.M. Carranza, M.G. Alvarez, Corros. Sci. 38 (1996) 909.
[36] M.G. Alvarez, A.M. Olmedo, M. Villegas, J. Nucl. Mater. 229 (1996) 93.
[37] M.F. Montemor, M.G.S. Ferreira, N.E. Hakiki, M. Da Cunha Belo, Corros. Sci. 42 (2000) 1635.
[38] N.S. McIntyre, R.D. Davidson, T.L. Walzak, A.M. Brennenstuhl, F. Gonzalez, S. Corazza, Corros. Sci. 37 (1995) 1059.

[39] M. Dupin, P. Gosset, Rapport EDF D5710/IMC/1999/005106/01.
[40] M. Dupin, P. Gosser, M.G. Walls, B. Rondot, J.-L. Pastol, S. Faty, M.G.S. Ferreira, M. Da Cunha Belo, Annales de Chimie Science des Matériaux 27 (2002) 19.
[41] C.M. Chen, K. Aral, G.J. Theus, Computer-calculated potential pH diagrams to 300 °C, Electric Power Research Institute Report EPRI-NP-3137, 1983.
[42] B. Beverskog, I. Puigdomenech, Corros. Sci. 39 (1997) 43.
[43] B. Beverskog, I. Puigdomenech, Corros. Sci. 39 (1997), 969.
[44] R.J. Lemire, G.A. McRae, J. Nucl. Mater. 294 (2001) 141.
[45] MULTEQ, The Database vol. 2, Electric Power Research Institute Report EPRI NP-5561-CCML, 1992.